Downloaded from rsif.royalsocietypublishing.org

JOURNAL OF THE ROYAL SOCIETY Interface

Human foetal osteoblastic cell response to polymer-demixed nanotopographic interfaces

Jung Yul Lim, Joshua C Hansen, Christopher A Siedlecki, James Runt and Henry J Donahue

J. R. Soc. Interface 2005 **2**, 97-108
doi: 10.1098/rsif.2004.0019

References This article cites 52 articles, 11 of which can be accessed free
http://rsif.royalsocietypublishing.org/content/2/2/97.full.html#ref-list-1

Email alerting service Receive free email alerts when new articles cite this article - sign up in the box at the top right-hand corner of the article or click **here**

To subscribe to *J. R. Soc. Interface* go to: **http://rsif.royalsocietypublishing.org/subscriptions**

This journal is © 2005 The Royal Society

Downloaded from rsif.royalsocietypublishing.org

JOURNAL OF THE ROYAL SOCIETY Interface

J. R. Soc. Interface (2005) **2**, 97–108
doi:10.1098/rsif.2004.0019
Published online 2 February 2005

Human foetal osteoblastic cell response to polymer-demixed nanotopographic interfaces

Jung Yul Lim[1], Joshua C. Hansen[2], Christopher A. Siedlecki[2,3], James Runt[4] and Henry J. Donahue[1,†]

[1]*Division of Musculoskeletal Sciences, Department of Orthopaedics and Rehabilitation, Center for Biomedical Devices and Functional Tissue Engineering, College of Medicine, The Pennsylvania State University, 500 University Drive, Milton S. Hershey Medical Center, Hershey, PA 17033, USA*
[2]*Department of Bioengineering, College of Medicine, The Pennsylvania State University, Hershey, PA 17033, USA*
[3]*Department of Surgery, Biomedical Engineering Institute, College of Medicine, The Pennsylvania State University, Hershey, PA 17033, USA*
[4]*Departments of Materials Science and Engineering and Bioengineering, The Pennsylvania State University, University Park, PA 16802, USA*

Nanoscale cell–substratum interactions are of significant interest in various biomedical applications. We investigated human foetal osteoblastic cell response to randomly distributed nanoisland topography with varying heights (11, 38 and 85 nm) produced by a polystyrene (PS)/polybromostyrene polymer-demixing technique. Cells displayed island-conforming lamellipodia spreading, and filopodia projections appeared to play a role in sensing the nanotopography. Cells cultured on 11 nm high islands displayed significantly enhanced cell spreading and larger cell dimensions than cells on larger nanoislands or flat PS control, on which cells often displayed a stellate shape. Development of signal transmitting structures such as focal adhesive vinculin protein and cytoskeletal actin stress fibres was more pronounced, as was their colocalization, in cells cultured on smaller nanoisland surfaces. Cell adhesion and proliferation were greater with decreasing island height. Alkaline phosphatase (AP) activity, an early stage marker of bone cell differentiation, also exhibited nanotopography dependence, i.e. higher AP activity on 11 nm islands compared with that on larger islands or flat PS. Therefore, randomly distributed island topography with varying nanoscale heights not only affect adhesion-related cell behaviour but also bone cell phenotype. Our results suggest that modulation of nanoscale topography may be exploited to control cell function at cell–biomaterial interfaces.

Keywords: cell–substratum interface; nanotopography; osteoblast; focal adhesion; nanobioscience

1. INTRODUCTION

Cells interact with the substrata they are growing on by secreting extracellular matrix (ECM) proteins. These ECM proteins in turn transduce extracellular signals, both chemical and physical, through the membrane to the cytosol via focal contacts (Hynes 1992; Giancotti & Ruoslahti 1999). This cell–ECM–substratum interaction is shared among cell ensembles via intercellular communication (Donahue 2000; Yap & Kovacs 2003), thus allowing for integration and amplification of extracellular signals. In this regard, cell–substrate interactions are critical to the integration and interpretation of extracellular signals by cell networks. Variations in substratum surface properties such as chemistry, topography, surface energy, etc., affect cell–biomaterial interfacial characteristics, potentially influencing cellular functions. This is an important consideration when developing novel materials for biomedical applications including prosthesis development and tissue engineering (Langer & Vacanti 1993). Thus, we examined the effect of substrate surface characteristics on osteoblastic cell behaviour.

We chose surface topography as a substrate characteristic to investigate because it has been shown that cell functions vary with the microtopographic features of substrata. For example, anisotropic topographies composed of ridges and grooves with varying width, depth and pitch, on the micrometre scale, have been extensively studied and demonstrated to induce cellular alignment and migration along the anisotropic direction (den Braber *et al.* 1996; van Kooten *et al.*

[†]Author for correspondence (hdonahue@psu.edu).

Received 25 August 2004
Accepted 5 November 2004

© 2005 The Royal Society

Downloaded from rsif.royalsocietypublishing.org

JOURNAL OF THE ROYAL SOCIETY Interface

1998; Flemming *et al.* 1999; Nealey 1999). Such 'contact guidance' has been reported for various cell types including fibroblasts, osteoblasts, epithelial cells and macrophages (Oakley & Brunette 1995*b*; Wojciak-Stothard *et al.* 1995; Walboomers *et al.* 1999; Matsuzaka *et al.* 2000). Development of focal adhesion proteins and organization of actin and tubulin cytoskeletal proteins have been positively correlated with contact-guided cellular orientation (Meyle *et al.* 1994; Britland *et al.* 1996; Oakley *et al.* 1997). Gene expression has also been reported to be altered by anisotropic microtopographies (Clark *et al.* 1987; Rajnicek & McCraig 1997). Thus, it is clear that microscale topography alters cell behaviour.

While microtopography affects cell behaviour, cells exist in interfaces with topography closer to the nanometre scale. For example, type-I collagen, the most abundant ECM protein in the body, forms fibrils with a repetitive cross-striation pattern every 67 nm (Alberts *et al.* 1994). Various tissues have basement membranes comprising a complex mixture of pores, protrusions, ridges and fibres having nanoscale sizes. The human corneal basement membrane has a rich felt-like topography with a dimension on the order of 20–200 nm (Teixeira *et al.* 2003), and the rat kidney basement membrane has a meshwork composed of fibrils approximately 10 nm thick and pores approximately 20 nm wide (Shirato *et al.* 1991). Despite increased awareness that cells exist on nanoscale topography, there have been few studies on the interaction of cells with nanoscale substratum topography (Clark *et al.* 1991; Wojciak-Stothard *et al.* 1996). However, rapid developments in nanofabrication technology using chemical, physico-chemical and electrical processes have made it possible to investigate cell–substratum interactions on the nanoscale. For example, epithelial cells were observed to display contact guidance on 70 nm wide ridges developed using electron-beam lithography (Teixeira *et al.* 2003). Fibroblasts were observed to respond differently on polystyrene/polybromostyrene (PS/PBrS) polymer-demixed topographies composed of nanoscale high islands (Dalby *et al.* 2002*b*, 2003, 2004*b*). Fibroblasts displayed increased adhesion and more developed cytoskeletons when they were cultured on surfaces with 13 nm high islands relative to surfaces with 95 nm high islands. However, this may be cell-line dependent in that rat calvarial osteoblastic cells did not display similar differences when cultured on similar PS/PBrS island nanotopographies (Riehle *et al.* 2003). Additionally, adhesion and cytoskeletal formation did not change in human primary osteoblastic cells cultured on TiO_2 covered with 110 nm high hemispheric protrusions at 3–43% protrusion coverage relative to flat TiO_2 substrata (Rice *et al.* 2003).

It is unclear whether the apparent cell-line dependent difference in responding to nanoscale topography is a general phenomenon or limited to specific cell lines, biological readouts or biomaterials. To address this issue, we investigated bone cell–nanotopographic substrata interactions by using a human foetal osteoblastic cell line, hFOB 1.19, cultured on polymer-demixed nanoisland topographies. The nanofabrication system we employed, PS/PBrS demixing, uses polymeric phase separation during a spin-casting process. The shape of the topographic features (holes, ribbons or islands) can be controlled by varying the composition of the polymer mixture and the size of a particular feature by varying the concentration of the spin-casting solution (Affrossman *et al.* 1996, 1998; Affrossman & Stamm 2000). The PS segments segregate preferentially to the film surface after annealing above the glass-transition temperature (T_g) of PS but below that of PBrS (Guckenbiehl *et al.* 1994; Affrossman *et al.* 1998; Dalby *et al.* 2002*a*), and cells consequently make contact with the PS component only. Thus, the effect of nanotopography can be assessed under the same surface chemistry. We examined hFOB cell morphology, dimension, lamellipodia and filopodia extension, cytoskeletal and focal adhesive protein synthesis, adhesion and proliferation. We also examined whether a specific bone cell phenotypic marker, alkaline phosphatase (AP) activity, was influenced by nanotopography. We demonstrated nanotopography-induced differential osteoblastic cell responses, not only with regard to adhesion-related cell behaviour but also bone cell phenotype.

2. MATERIALS AND METHODS

2.1. hFOB cell culture

hFOB cells were subcultured in DMEM-Ham's F-12 1:1 media (GIBCO) supplemented with 10% foetal bovine serum (FBS, Hyclone) and 1% penicillin–streptomycin on tissue culture polystyrene (TCPS) and incubated at 37 °C in a standard incubator with 5% CO_2 in air. Prior to culture on test substrata, cells were removed from TCPS by rinsing in phosphate-buffered saline (PBS) and incubating in trypsin–EDTA solution, and seeded in the same complete media. Cells were allowed to adhere for 3 h on each test substrata, rinsed with PBS, and the remaining adherent cells were either subjected to assays immediately or allowed to proliferate for specific times, with media changed every 3 days.

2.2. Nanotopographic substrata and characterization

Randomly distributed nanoisland topography was produced by PS/PBrS polymer demixing (Riehle *et al.* 2003; Dalby *et al.* 2004*b*). The PS ($M_w = 289 \times 10^3$) and PBrS ($M_w = 65 \times 10^3$) were purchased from Aldrich. The PS/PBrS mixture (40/60, w/w) was dissolved in toluene, and the total polymer concentration adjusted to 0.5, 2 and 5% (w/w) to produce three different feature heights. Spin-casting of polymer solutions onto monolithic quartz substrate was performed at 4000 r.p.m. for 30 s using a Spincoater (speciality coating system). Before spin-casting, the quartz substrate was plasma-treated after consecutive washing in distilled water, isopropyl alcohol and chloroform. Spin-cast, polymer-demixed films were dried for 24 h at room temperature and annealed above the T_g of PS (103 °C) but below the T_g of PBrS (150 °C). Films spin-cast from 0.5% solution were annealed for 1 h at 110 °C, and those

Downloaded from rsif.royalsocietypublishing.org

spin-cast from 2 and 5% solutions for 2 h at 130 °C. For flat controls, PS and PBrS homopolymer films were produced from a 5% (w/w) toluene solution by using the same spin-casting conditions but without annealing. For sterilization, all of the test substrata were treated under ultraviolet light for 1 h before cell seeding.

Surface topography of demixed PS/PBrS and control PS and PBrS films was assessed by using atomic force microscopy (AFM; Nanoscope IIIa, Digital Instruments) in TappingMode under ambient conditions. Three samples per substratum were characterized. For each sample, at least six random spots, including the centre and regions toward the edge, were analysed to assess the uniformity of the substrate and to determine the average height of the features. Additionally, percentage cover of the islands per unit surface area was determined. The water wettability of test substrata was assessed by measuring the water contact angle using a contact angle goniometer, G10 (KRÜSS). Double-distilled water (10 µl) was dropped on films and after 5 min the static contact angle was monitored. Water adhesion tension (τ) was calculated from the water contact angle (θ) by $\tau = \gamma \cos\theta$, where γ is the surface tension of water, 72.8 dyne cm^{-1} (Vogler 1999). Means and standard deviations ($n=7$) are reported for wettability.

2.3. Scanning electron microscopy (SEM)

hFOB cell morphology on nanoislands and flat substrata was assessed with a FEI-Philips XL-20 scanning electron microscope. Cells were seeded at 8×10^3 cells cm^{-2} on each test substrata for 3 and 24 h and the unattached cells were removed by rinsing with PBS. Adherent cells were fixed for 20 min at room temperature in a 2.5% glutaraldehyde solution in PBS. Fixed cells were washed with PBS and dehydrated by adding, successively, a graded series of ethanol/distilled water mixtures containing 50, 80, 90, 95, 98 and 100% ethanol, for 10 min at each stage. Dehydrated cells were dried at room temperature. For SEM measurement, samples were sputter-coated with gold and observed at an accelerating voltage of 20 kV. At least 15 cells per condition were characterized.

2.4. Quantification of cell morphology

Cell morphology on each test substrata was assessed by quantifying cell area, perimeter, Feret's diameter (length from tip-to-tail of the cell), circularity and coverage per unit substratum surface area. Cells were seeded at 1.2×10^4 cells cm^{-2} and, after culturing of 3 h, cells were washed with PBS and fixed with 4% paraformaldehyde in PBS for 20 min. Fixed cells were then stained for 2 min with 0.5% Coomassie blue aqueous solution containing methanol/glacial acetic acid, washed with water to remove excess dye and then observed using a light microscope. Shape parameters of cells were quantified using image-analysis software, ImageJ, from the United States National Institutes of Health (http://rsb.info.nih.gov/nih-image/). ImageJ automatically detects the cell outline and calculates shape parameters based on the number of pixels covered by the cell. Actual pixel dimension was calibrated using a stage micrometer. Experiments were repeated twice to take images of a total of nine different random spots of 720×960 µm^2 size at a $10\times$ objective magnification (under $10\times$ eyepieces). Means and standard deviations of nine measurements are reported, each containing 25–50 cells. When cells were found to be clustered with other cells, they were manually excluded from datasets. A total of 200–400 cells were analysed per substrata.

2.5. Immunofluorescence assay

Synthesis of actin and vinculin proteins by hFOB cells was observed by immunofluorescent staining. Cells were seeded at 1.2×10^4 cells cm^{-2} on each test substrata. After culturing for 3 and 24 h, cells were washed with PBS three times and fixed with 4% paraformaldehyde in PBS for 20 min. Fixed cells were rinsed with PBS and permeabilized for 5 min with 0.1% Triton X-100 (Sigma) in PBS. After rinsing with wash buffer made of PBS with 0.05% Tween-20 (Sigma), cells were pre-incubated for 30 min at room temperature with 1% bovine serum albumin (BSA, Sigma) in PBS to minimize non-specific protein–protein interactions. After washing, cells were exposed for 1 h at room temperature to murine monoclonal antivinculin (Chemicon, FAK100 kit-90227) solution in PBS (1:100) with 1% BSA. After rinsing three times, cells were incubated for 1 h at room temperature with fluorescein isothiocyanate (FITC)-conjugated goat anti-mouse IgG secondary antibody (Chemicon, AP124F) solution in PBS (1:50) with 1% BSA. To detect actin simultaneously, cells were double-labelled with tetramethylrhodamine isothiocyanate (TRICT)-conjugated phalloidin (Chemicon, FAK100 kit-90228; 1:250) using the same vinculin secondary antibody solution. Immunoreactivity of actin and vinculin was observed at a $40\times$ objective magnification (under $10\times$ eyepieces) using a Nikon OPTIPHOT-2 fluorescent microscope with filters appropriate for TRITC and FITC.

2.6. Adhesion and proliferation assays

Adhesion and proliferation of hFOB cells on test substrata were assessed by counting cell number using a haemacytometer. For adhesion tests, cells were seeded at 1.5×10^4 cells cm^{-2} and allowed to attach to each substrata. After 3 h, non-adherent cells were removed by washing with PBS three times and adherent cell number was determined with a haemacytometer. For proliferation assays, cells were seeded at the same density and allowed to adhere. After 3 h, cells were rinsed with PBS, and the adherent cells were allowed to proliferate for 3, 6 and 9 days with media changed every 3 days. Each day, substrata were rinsed with PBS and cell number counted with a hemacytometer. Both adhesion and proliferation assays were conducted three times, each in triplicate samples.

2.7. AP activity

AP activity of hFOB cells cultured on nanoislands and flat substrata was quantified at 3, 6 and 9 days. Cells were cultured in the same fashion as for the

Downloaded from rsif.royalsocietypublishing.org

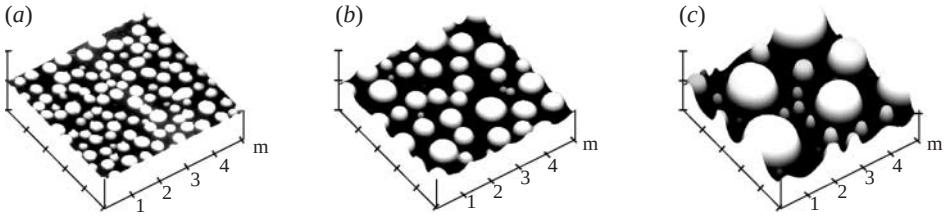

Figure 1. AFM images of PS/PBrS polymer-demixed nanotopographies with varying average island height: (*a*) 11 nm, (*b*) 38 nm and (*c*) 85 nm. All images are shown at the same scale ($5\times5\ \mu m^2$ size with *z*-scale of 150 nm per division).

proliferation assay, and AP activity quantified using a chromogenic assay involving conversion of *p*-nitrophenyl phosphate to *p*-nitrophenol. Cells were rinsed with PBS and lysed with Triton X-100. Cell lysates were subjected twice to freeze–thaw cycles, after which an AP reaction buffer of a 1:1 mixture of 0.75 M 2-amino-2-methyl-1-propanol (Sigma A9226) and $2\ mg\ ml^{-1}$ *p*-nitrophenol phosphate (Sigma 104-40T) was added. This reaction mixture was combined with 0.1 N NaOH in a 96-well plate and incubated at 37 °C for 15 min. The absorption was measured at 410 nm, and enzyme activity was estimated from a *p*-nitrophenol standard curve. The AP activity was obtained by normalizing the enzyme activity to the total protein amount, which was measured using a detergent compatible protein assay kit (Bio-Rad). Three different cultures were conducted for AP activity measurement, each comprising three substrates.

2.8. Statistics

Means and standard deviations are reported. Statistical significance between groups was assessed by one-way analysis of variance (ANOVA) followed by Student–Newman–Keuls *post hoc* multiple comparison tests. Comparisons with the flat PS control (* and **) as well as comparison among nanoisland substrata (# and ##) are presented (see figure 5 for details).

3. RESULTS

3.1. Nanoislands with varying heights

Spin-casting films with 40/60 (w/w) PS/PBrS composition resulted in nanoisland topography. The island height was controlled by the spin-casting solution concentration, i.e. 0.5, 2 and 5% (w/w) concentration produced average island heights of 10.8 ± 1.4, 38.2 ± 4.8 and 84.9 ± 11.7 nm, respectively, as measured by AFM. In this study, we refer to nominal heights of 11, 38 and 85 nm. These results are similar to those reported previously (Riehle *et al.* 2003; Dalby *et al.* 2004*b*). Representative AFM images (figure 1) reveal the random spatial distribution of the nanoislands. With increasing island height, individual island area increased and the area distribution became less uniform. For example, islands with mostly small areas were observed on surfaces consisting of 11 nm features, but both large- and small-area islands were observed on surfaces with 85 nm features. For 85 nm high surfaces, large-area islands were found to be 95–100 nm high while islands with smaller areas were 70–75 nm high. The surface fraction covered by islands was not significantly different ($p>0.05$) among the three nanoisland substrata ($37.3\pm2.3\%$ for 11 nm, $38.3\pm3.1\%$ for 38 nm and $36.2\pm2.8\%$ for 85 nm surfaces). The actual change in surface area including island sidewalls was not assessed. Spin-cast films of PS and PBrS only displayed a flat topology with no identifiable features (not shown). Island nanotopography can be also seen in SEM images (figures 2 and 3).

3.2. Nanotopography-dependent lamellipodia and filopodia development

Cells on surfaces with 11 nm high nanoislands displayed well-developed lamellipodia and thus enhanced cell spreading for both 3 and 24 h of culturing (figure 2*a*,*b*). Cell spreading was less pronounced for island heights of 38 and 85 nm (figure 2*c*–*f*). On 85 nm island surfaces, cells often displayed a stellate cell shape with filopodia extending from the stellate legs (figure 2*f*). Cells on the flat PS control developed less distinct lamellipodia, while cells on flat PBrS displayed well-developed, highly spread lamellipodia.

Higher magnification SEM images for 24 h culture more clearly reveal the lamellipodia and filopodia development. Cells on 11 nm island surfaces displayed ruffles at the leading lamellipodia edge (figure 3*a*), while cells on 85 nm surfaces displayed filopodia extensions at the growing fronts (figure 3*c*). Cells on 38 nm surfaces displayed a rather intermediate morphology with attenuated (relative to cells on 11 nm surfaces) lamellipodia spreading with protruding filopodia (figure 3*b*). Lamellipodia and filopodia appear to interact with both the top and other portions of nanoislands. Additionally, lamellipodia appear not to bridge the nanoislands but rather display a topography-conforming morphology that mimics the nanoislands for all three nanoscales (figure 3*a*,*b*,*e*).

Time-dependent lamellipodia and filopodia formation on 85 nm nanoisland surfaces is shown in figure 3*d*–*f*. We often observed that cells cultured for 3 h on 85 nm surfaces were still in the early stages of adhesion (sedimentation and initial contact), which was not the case for smaller island surfaces. In this early stage, cells first interact with the surface by extending filopodia and touching both top and other portions of nanoislands (figure 3*d*). Initially, filopodia appear to interact mostly with the top parts of islands. Some cells reached a later stage of adhesion (spreading) at 3 h (figure 3*e*), where lamellipodia extension and filopodia projection from the leading edge were observed. At 24 h, most cells displayed

Downloaded from rsif.royalsocietypublishing.org

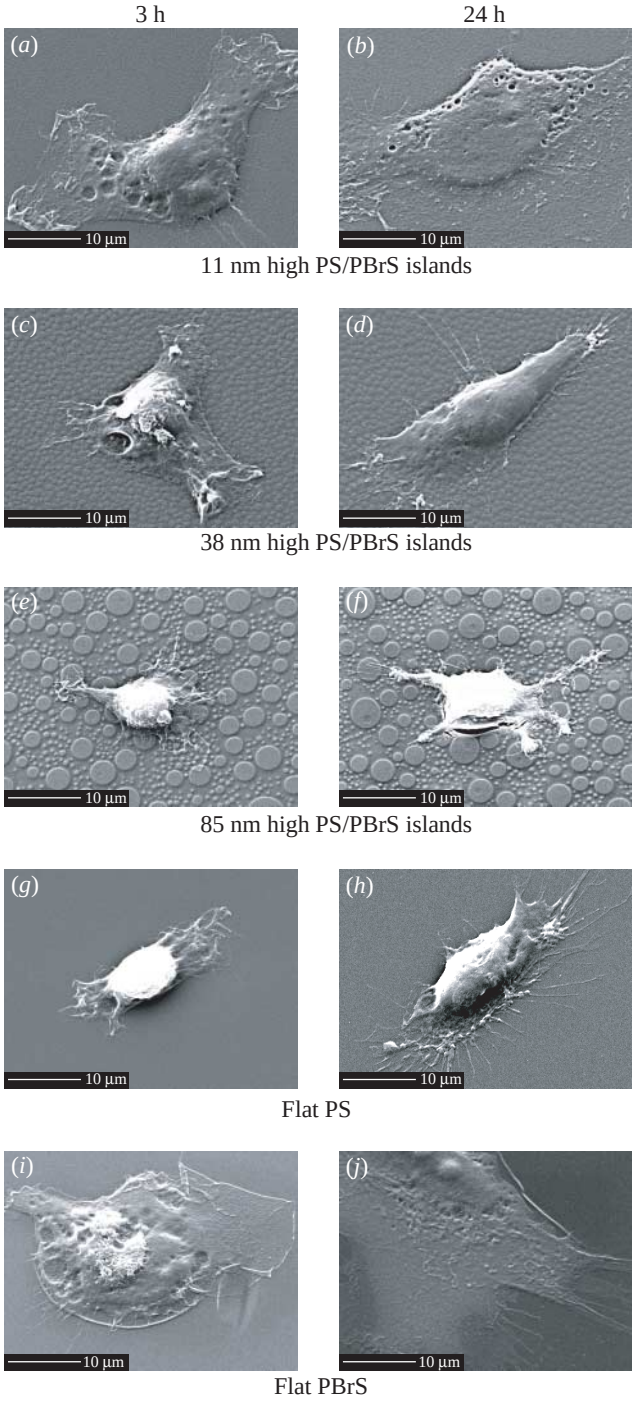

Figure 2. SEM images of hFOB cells cultured for 3 h (*a*), (*c*), (*e*), (*g*) and (*i*) or 24 h (*b*), (*d*), (*f*), (*h*) and (*j*) on nanoislands and flat substrata. Substrata notation and scale bar are indicated in the figure.

lengthy filopodia extensions (figure 3*f*). Once the spreading stage was achieved, topography-conforming lamellipodia growth was seen (figure 3*e*,*f*). Not all the filopodia formed up and down on the nanoislands but, rather, some filopodia extended along the circumferential direction of the islands (figure 3*f*).

3.3. Cells on 11 nm high nanoislands display larger cell dimensions but lower circularity

Coomassie blue stained images also reveal that cells were less well-spread and often displayed a stellate shape with increasing island height (figure 4*a*–*c*). On the flat PS control, cells displayed various shapes including stellate. On the flat PBrS surface, cells displayed a more well-spread shape and the highest degree of attachment. These results are summarized in figure 5. Compared with cells on the flat PS, cells cultured on 11 nm island surfaces and on the flat PBrS exhibited a significantly larger cell area, perimeter and Feret's diameter. Among the nanotextured surfaces, cells on 11 nm surfaces displayed significantly larger cell dimensions compared with cells on 38 and 85 nm surfaces. Cells on 38 and 85 nm surfaces and flat PS did not exhibit significant differences in cell dimensions, except for a smaller Feret's diameter for cells on 85 nm surfaces relative to cells on the flat PS. Circularity was greater when cell spreading was suppressed (on 85 nm surfaces), but lower when cell spreading was enhanced (on 11 nm surfaces and the flat PBrS). Coverage per unit surface area was similar to the area results for individual cells.

3.4. Cells on smaller nanoislands display well-developed actin stress fibres and vinculin

The development of actin and vinculin proteins in hFOB cells was different on surfaces with nanoislands of different height (figure 6). Cells on 11 nm surfaces displayed actin stress fibres and vinculin plaques after 3 h of culture, whereas cells on 38 and 85 nm surfaces displayed more diffused actin and vinculin immunoreactivity (figure 6*a*,*b*,*e*,*f*,*i*,*j*). After 24 h of culture, highly tensioned actin stress fibres and distinct vinculin plaques were apparent within cells on 11 nm surfaces, beginning to develop within cells on 38 nm surfaces but undeveloped within cells on 85 nm surfaces (figure 6*c*,*d*,*g*,*h*,*k*,*l*). Colocalization of actin and vinculin proteins became distinct after culturing for 24 h but only within cells on surfaces with 11 nm islands. For these cells, the rapidly growing plus ends of actin fibres inserted into the leading edge of the plasma membrane, while the other ends terminated at or close to vinculin plaques (figure 6*c*,*d*). Actin stress fibres and vinculin plaques were poorly developed on the flat PS control, similar to the cells on surfaces with larger nanoislands. However, cells on the flat PBrS displayed well-developed actin stress fibres and vinculin plaques as well as their colocalization, similar to the cells on 11 nm surfaces.

3.5. Cells on smaller nanoislands display a systematic increase in adhesion and proliferation

Cell adhesion at 3 h was greatest on 11 nm surfaces among the nanoisland substrata and decreased with increasing island height (figure 7*a*). Relative to cell adhesion on flat PS, cell adhesion was greater on 11 nm, similar on 38 nm but lower on 85 nm island surfaces. On two flat samples, cells adhered more to relatively hydrophilic PBrS compared with relatively hydrophobic PS (figure 7*b*). This was also the case for hFOB cell spreading on PBrS and PS, and this result is similar to endothelial cell spreading on PS and PBrS

Downloaded from rsif.royalsocietypublishing.org

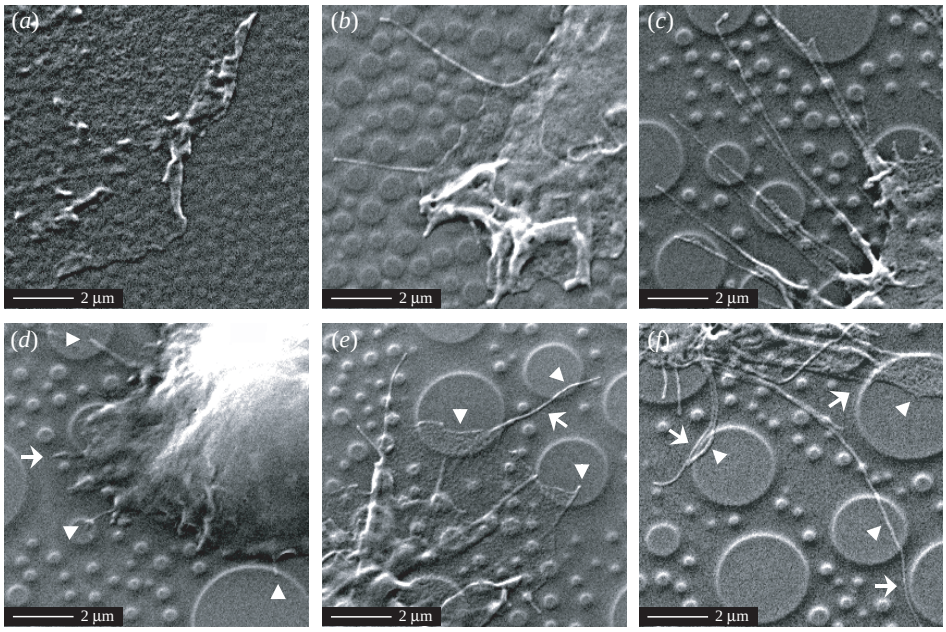

Figure 3. High-magnification SEM images of hFOB cells cultured for 24 h on surfaces with (*a*) 11 nm, (*b*) 38 nm and (*c*) 85 nm surfaces. Additional examples of hFOB cells cultured on 85 nm substratum are shown after 3 h ((*d*),(*e*)) and 24 h (*f*) of culture. Arrowhead and arrow indicate the interaction with top and other portions of island topography, respectively. Scale bars indicated.

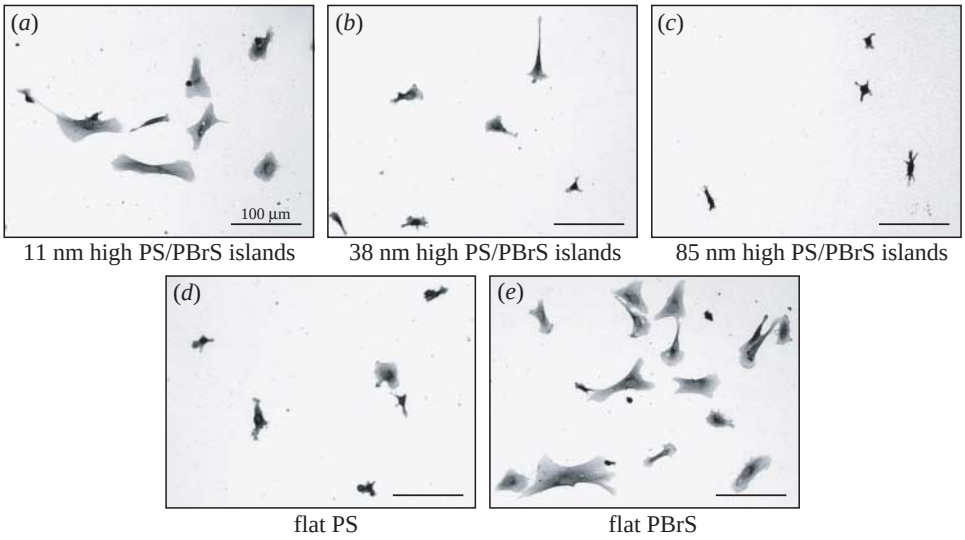

Figure 4. Coomassie blue stained hFOB cells cultured for 3 h on nanoislands and flat substrata. Original 720×960 µm^2 size images were taken at a 10× objective magnification and used for image analysis of cell dimensions. Cropped sample images (360×480 µm^2) are shown with substrata notation and scale bar.

flat surfaces (Dalby *et al.* 2002*a*). Contact-angle measurements reveal that nanotopography can induce wettability changes (figure 7*b*), while the same surface chemistry of PS is maintained. In general, cell adhesion and spreading on nanoisland or flat surfaces were correlated with surface water wettability. For example, the smaller the nanoislands, the smaller the water contact angle, and, accordingly, cells adhered more. However, there are some exceptions, e.g. surfaces with 38 nm islands and the flat PS exhibit different water wettability but similar adhesion. Cell proliferation for 3, 6 and 9 days displayed a similar variation on substrata, as did cell adhesion (figure 8).

3.6. Cells on nanotextured surfaces display different AP activity

Substrate-dependent AP activity demonstrated that bone cell phenotype may also be affected by surface nanotopography (figure 9). hFOB cells cultured on all of the test substrata displayed low and statistically invariant AP activity up to day 6. AP activity increased significantly on day 9 and exhibited substrate-dependent variation. hFOB cells cultured on 11 nm surfaces displayed higher AP activity than did cells on the flat PS control or on 38 and 85 nm surfaces. hFOB cells cultured on 38 and 85 nm islands and flat

Downloaded from rsif.royalsocietypublishing.org

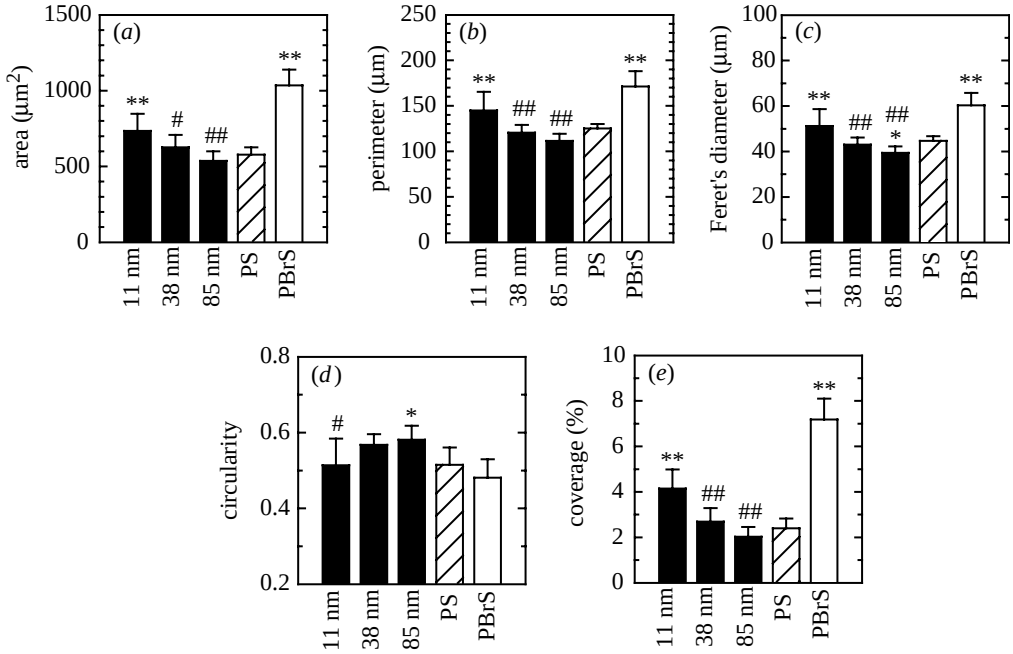

Figure 5. hFOB cell dimensions after 3 h of culturing on nanoislands and flat substrata analysed by ImageJ software: (*a*) area, (*b*) perimeter, (*c*) Feret's diameter, (*d*) circularity and (*e*) percentage coverage per unit substratum surface area. Statistical significance examined by ANOVA followed by Student–Newman–Keuls *post hoc* multiple comparison test is shown. When compared with the flat PS control, statistical significance is denoted by * ($p<0.05$) and ** ($p<0.01$). When compared among nanoisland substrata, it is denoted by # ($p<0.05$) and ## ($p<0.01$), where the nanoisland substratum displaying the highest value is set as the control for the individual parameter. For example, the 11 nm substratum was set as the control for area, perimeter, Feret's diameter and coverage, and the 85 nm substratum for circularity.

PS displayed similar AP activities, while cells on the flat PBrS displayed higher AP activity than those on the flat PS. While cell proliferation varied with respect to substrata for the entire culture period up to 9 days, AP activity varied only after sufficient cell proliferation was achieved, on day 9. Even though the 85 nm surfaces were less supportive of hFOB adhesion and proliferation than the flat PS control, hFOB cells cultured on 85 nm surfaces displayed similar AP activity as those on the flat PS.

4. DISCUSSION

We hypothesized that nanotopography composed of randomly distributed islands with varying nanoscale heights induces a differential osteoblastic response at cell–biomaterial interfaces. Our results suggest that various aspects of bone cell behaviour are indeed systematically affected by substratum nanotopography. This includes not only adhesion-related cell responses but also bone cell phenotype.

The surface topography investigated in this study can be classified as isotropic, relative to the anisotropic nature of a ridge-and-groove texture. The random spatial distribution of islands brings about uniformly distributed, isotropic nanotopography. Island coverage per unit surface area is similar for all three island heights, even though island number and area are different. We measured the heights of islands to characterize nanoscales. Recalling the isotropic nature of randomly distributed nanoisland topography, it is perhaps not surprising that we did not observe contact guided cell alignment. However, we did see differential bone cell responses with respect to nanotopographic scales as regards cell attachment and proliferation, focal adhesion and cytoskeletal protein synthesis and bone cell phenotype.

Previous investigations of cell–topography interactions have focused on whether cells conform to, or bridge, topographic features. This is mainly because, in addition to affecting cell shape, conforming or bridging directly affects the formation of focal contact. In this study, hFOB cells appeared to conform to the nanoisland topography up to approximately 100 nm scales as seen by island-mimicking spread of lamellipodia (figure 3*a*,*b*,*e*). While there have been no reports of such lamellipodia spreading on isotropic protrusions, it has been reported that the ability of cells to descend into grooves and form focal adhesions on groove floors increases with increasing groove width and decreasing groove depth (Walboomers *et al.* 1998, 1999). These results were reported for groove depths ranging from several μm down to 500 nm. Recently, epithelial cells were found to descend into 2100 nm wide grooves with depths of 600 and 150 nm (Teixeira *et al.* 2003). However, those cells formed bridges between ridges when groove width was 950–330 nm, for the same groove depths. These results and those of this study suggest that the topographic feature height above which lamellipodia growth becomes selective between bridging or conforming may lie above approximately 100 nm (large islands on 85 nm high substrate are 95–100 nm high).

When cells spread, move or change shapes, they extend lamellipodia, protrude microspikes and filopodia at their leading edge, or leave retraction fibres after cell withdrawal. All these cellular processes are motile and involved in local actin polymerization (Alberts

Downloaded from rsif.royalsocietypublishing.org

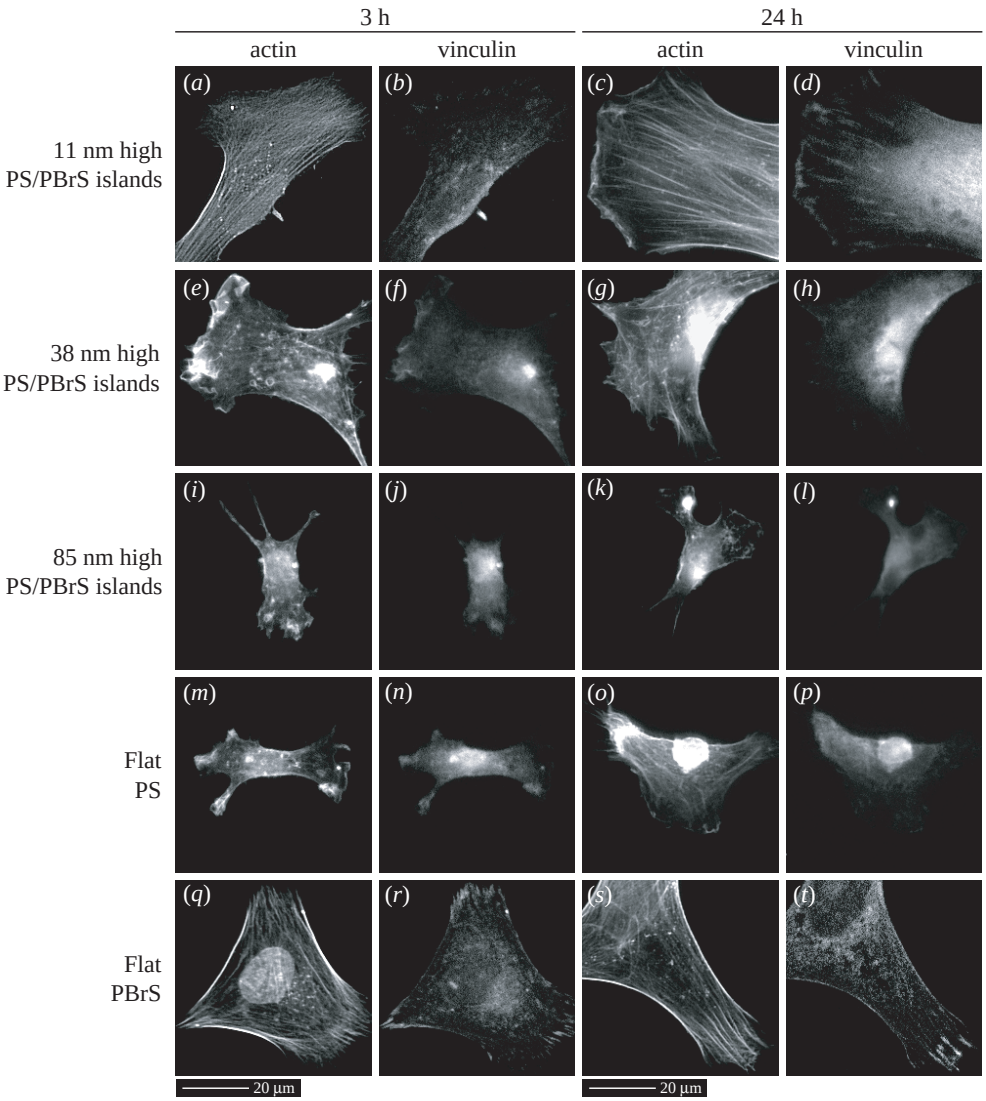

Figure 6. Actin and vinculin double-labelled immunofluorescence images of hFOB cells cultured for 3 and 24 h on nanoislands and flat substrata taken at a 40× objective magnification. Substrata notation and scale bars are indicated. Distinct actin stress fibres and vinculin plaques as well as their colocalization were seen in cells cultured on 11 nm high nanoisland surfaces ((*c*), (*d*)), while more diffused actin and vinculin immunoreactivities on larger nanoisland substrata ((*k*), (*l*)).

et al. 1994). Recently, it was observed by time-lapse microscopy that microspikes, filopodia and retraction fibres (all have similar structure of actin bundles) are interconvertible with cycles of lamellipodia protrusion and withdrawal (Svitkina *et al.* 2003). Depending on the advancing velocity of lamellipodium relative to the actin bundle elongation, the bundle appears as a microspike (if inserted inside the lamellipodium) or a filopodium (if protruded outside it). If the lamellipodium withdraws while the actin bundle remains stable or elongated, the bundle appears as a retraction fibre. In this study, all these types of actin bundles were referred to collectively as 'filopodia', as was the case in the study by Svitkina *et al.* (2003). It has been proposed that filopodia play a role in cell recognition of the substratum topography, since filopodia protrude at the foremost front of the cell. Filopodia sensing was suggested to be important in contact-guided epithelial cell orientation based on the observation that filopodia displayed an active interaction with topographic features and were frequently aligned in the anisotropic direction (Teixeira *et al.* 2003). The role of filopodia sensing of nanoscale topography was recently demonstrated on substrata with 10 nm high protrusions (Dalby *et al.* 2004*c*) and 35 nm diameter pits (Dalby *et al.* 2004*a*). Our results add additional evidence of this phenomenon. When cells attach to nanoislands, they first contact the surface by filopodia extending and touching the top and other portions of the nanoislands (figure 3*d*). Some filopodia extend either along the edges of 85 nm high nanoislands or form projections pointing up and down the islands (figure 3*f*).

hFOB cells cultured on surfaces having 11 nm high islands were well spread, relative to those on larger islands or flat PS control, on which cells often displayed a less-well-spread stellate shape (figures 2–4). Thus, cell dimensions were significantly larger on 11 nm surfaces (figure 5). Also, cell adhesion increased continuously with decreasing island height, and proliferation was adhesion dependent (figures 7*a* and 8). We conclude that the effect of nanoisland topography on various adhesion-related cell behaviours is systematic and

Downloaded from rsif.royalsocietypublishing.org

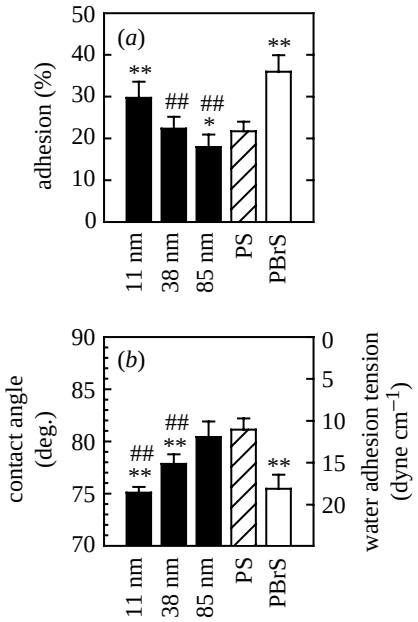

Figure 7. (*a*) hFOB cell adhesion after 3 h of culturing on nanoislands and flat substrata. (*b*) Water contact angle (θ) and water adhesion tension (τ), calculated from $\tau = \gamma \cos\theta$, where γ is water surface tension (72.8 dyne cm^{-1}), of each substrata are shown in. Notations for statistical significance are the same as in figure 5. hFOB cell adhesion was greater on surfaces with smaller islands ($p<0.01$ for 11–38 nm and $p<0.05$ for 38–85 nm island comparisons). Compared with the flat PS control, adhesion was improved on 11 nm ($p<0.01$), similar on 38 nm but lowered on 85 nm island substrata ($p<0.05$). The relatively hydrophilic, flat PBrS surface was more highly supportive of hFOB cell adhesion compared with the hydrophobic flat PS ($p<0.01$).

consistent, except that cells on 38 and 85 nm surfaces display significant differences in adhesion and proliferation but not in cell dimensions. These findings for hFOB cells are similar to those previously reported for fibroblast interactions with nanoislands (Dalby *et al.* 2002*b*, 2003, 2004*b*), but quite different from rat calvarial bone cell response to similar surface topography (Riehle *et al.* 2003). Rat calvarial osteoblasts adhered better on larger nanotopographic scales at short culture periods of 1 and 4 h. Rat calvarial osteoblasts did not otherwise display dramatic changes in cell behaviour including focal adhesion formation. However, we showed that hFOB cells adhere and proliferate better on smaller nanoscale surfaces and that they displayed significant differences in focal adhesion assembly with respect to nanotopographies. It is unclear why two bone cell types are affected differently by nanoscale topography. One possibility is that primary cultured rat calvarial bone cells have intrinsically less ability of adhesion and proliferation (Riehle *et al.* 2003) and thus may show minimal variation with respect to substratum surface characteristics relative to a rapidly proliferating hFOB cell line (Harris *et al.* 1995).

Focal adhesion and cytoskeleton formation were also affected by substratum nanotopography (figure 6). hFOB cells cultured on smaller nanoisland surfaces displayed more mature vinculin plaques and highly tensioned actin fibres, as well as colocalization, relative to cells on larger nanoisland surfaces and the flat PS control. In parallel, cell spreading, adhesion and proliferation displayed similar trends with respect to nanotopography, which supports the concept that focal adhesion structure development at cell–biomaterial interfaces is closely related to cell adhesion and further cell function. Several studies have examined whether focal adhesion formation is a prerequisite for cell-morphology variation. It is generally accepted that development of cytoskeleton–focal adhesion complexes occur simultaneously with changes in cell morphology, both affecting one another (Oakley & Brunette 1995*a*; Ezzell *et al.* 1997; Chen *et al.* 2003). This may also be the case for osteoblastic cells on nanotopography. For instance, enhanced lamellipodia spreading on smaller nanoisland surfaces occurred in parallel with formation of stressed actin filaments and their anchors (vinculin plaques). More importantly, the finding that signal transmitting structures (e.g. vinculin–actin) are differentially regulated on nanotopographies strongly suggests that cellular functions, especially mechanotransduction, may be controlled by the modulation of substratum topography at the nanoscale.

Pre-treatment of ECM proteins on the substrate can regulate cell behaviour by altering focal adhesion. For example, fibronectin and vitronectin coating of substrates selectively induces binding with integrins $\alpha_5\beta_1$ and $\alpha_v\beta_3$, respectively, at focal contacts (Moursi *et al.* 1997; Lacouture *et al.* 2002). It has also been reported that pre-coating density differences of arginyl-glycyl-asparatic acid (Arg-Gly-Asp, RGD) sequences bring about gradient focal adhesion formation and cell spreading (Massia & Hubbell 1991). In contrast, our results indicate that the substratum *per se*, without ECM pre-treatment, but on to which cells secrete ECM after they have attached, can regulate focal adhesion and cytoskeletons by nanoscale topography modification. However, it is possible that nanoscale topography is affecting the ability of serum compounds to adhere which then affects subsequent cell adhesion. This possibility is supported by our preliminary findings that in the absence of serum nanotopography does not as dramatically affect cell adhesion. Thus, while it is clear that nanoscale topography affects cell adhesion, it is not clear whether this is a direct effect on cells or indirect via an effect on serum component adsorption.

Water wettability of biomaterials is affected by various factors (Al-Omari *et al.* 2001). Surface energy of the biomaterial, which varies as a function of chemical composition and net polarity, strongly influences wettability. Additionally, surface topography influences wettability. Surface irregularities are presumed to enhance the wettability by producing increased surface area (Al-Omari *et al.* 2001). In this case, the 'effective' contact angle is lower on textured surfaces relative to flat surfaces as the surface roughness is impregnated (Bico *et al.* 2001). On the contrary, excessive roughness may result in air being trapped at the interface causing ultra-hydrophobicity, i.e. higher contact angles (Öner & McCarthy 2000). Our results showing that nanotextured surfaces decrease contact

Downloaded from rsif.royalsocietypublishing.org

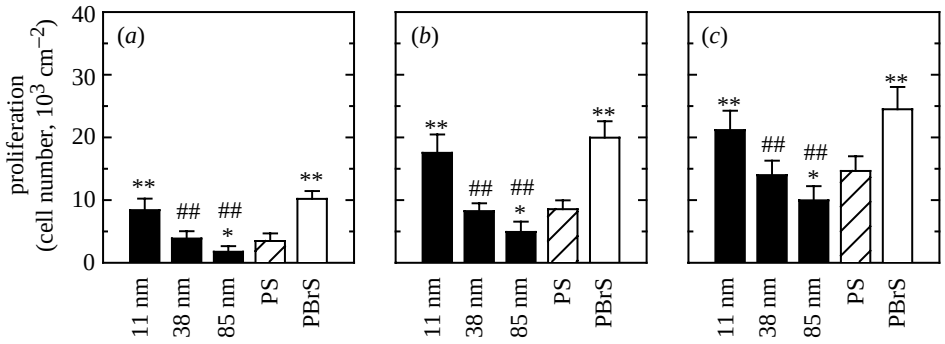

Figure 8. hFOB cell proliferation after (*a*) 3, (*b*) 6 and (*c*) 9 days of culturing on nanoislands and flat substrata. Notations for statistical significance are the same as in figure 5.

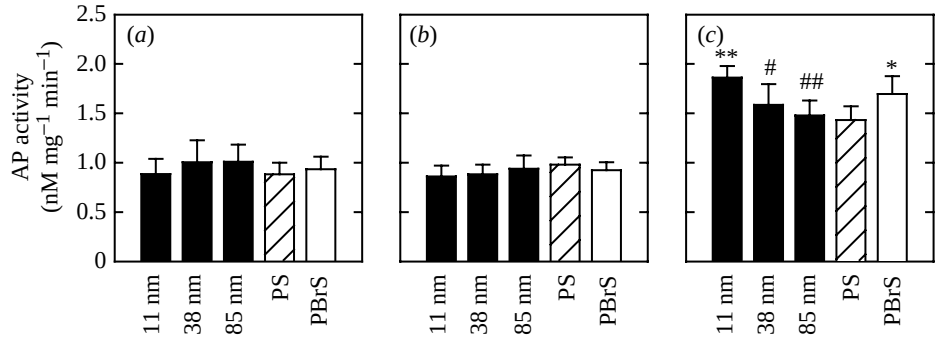

Figure 9. AP activity in hFOB cells after (*a*) 3, (*b*) 6 and (*c*) 9 days of culturing on nanoislands and flat substrata. Notations for statistical significance are the same as in figure 5. On day 9, hFOB cells on 11 nm high island surfaces displayed higher AP activity than did cells on the flat PS control ($p<0.01$), 38 nm island ($p<0.05$) and 85 nm islands ($p<0.01$). Cells cultured on 38 and 85 nm islands and flat PS had similar AP activities on day 9.

angles is an example of the former case. We previously investigated the effect of substratum surface energy on bone cell behaviour by using various flat substrata, including bioabsorbable polymers, covering the entire range of biomaterials water wettability ($0°<\theta<120°$). We observed a systematic correlation in hFOB adhesion and proliferation with substrate wettability, i.e. the more hydrophilic (lower θ, higher τ), the greater the hFOB adhesion and proliferation (Lim *et al.* 2004). We further observed that hFOB cells cultured on fully wettable substrata ($\theta=0°$) were well spread and displayed distinct actin stress fibres colocalized with $\alpha_v\beta_3$ integrin and vinculin at focal contacts. Those cells displayed higher expression of α_v and β_3 integrin subunits and vinculin in Western blot analysis relative to cells grown on poorly wettable substrata ($\theta\sim120°$; Lim *et al.* 2005). The results of the current study are similar in that water wettability altered by nanotopography was related to cell adhesion, spreading, proliferation and development of actin–vinculin, similar to our previous studies.

In addition to influencing wettability, there may be more direct effects of nanoscale topography on cell behaviour. This is based on our finding that cells adhered similarly to surfaces with different contact angles (e.g. 38 nm islands versus flat PS) and differently to surfaces with similar contact angles (e.g. 85 nm islands versus flat PS; figure 7). Thus, cross-comparison between nanotextured and flat surfaces was not always consistent. Also, changes in contact angle observed herein for textured surfaces were smaller than those of our previous studies on surface wettability ($0°<\theta<120°$). This suggests that topography can affect bone cell behaviour independent of water wettability. As pointed out earlier, surface roughness can interfere with protein adsorption, which will in turn affect cell behaviour. Also, cells themselves are strongly influenced by the respective surface roughness and wettability they face when they arrive at the cell–biomaterial interface (Rupp *et al.* 2004).

Control of cell phenotypic expression by substratum characteristics is also critically important in tissue engineering, where controlled expression and maintenance of target cell phenotype is essential for successful cell growth *in vitro* (Boyan *et al.* 1996). In this regard, AP activity variation provides evidence that bone cell differentiation is also affected by substratum nanotopography (figure 9). The variation in AP activity on nanoisland substrata was observed after the proliferation period and generally followed adhesion-related cell behaviour. An exception was that AP activity on larger nanoisland (85 nm) surfaces was comparable to that on flat PS, even though adhesion and proliferation on larger islands surfaces were suppressed relative to flat PS. AP activity is regarded as a relatively early stage bone cell phenotype. AP activity in hFOB cells cultured on TCPS was detected after a relatively short culture period (maximum on day 6), followed by the later stage (1–2 weeks or more)

Downloaded from rsif.royalsocietypublishing.org

expression of other bone cell phenotypic markers such as osteocalcin and osteopontin (Donahue *et al.* 2000). Thus, we conclude that hFOB cells respond systematically to nanoisland topography during early stages of cell growth (3 h to 6–9 days). Whether long-term bone cell phenotypes, including mineralization, are affected by the nanotopography is currently being examined.

In conclusion, osteoblastic cells respond differentially to nanoscale topographies composed of randomly distributed islands with height varying between 11 and 85 nm. The fact that osteoblastic cells adhere differentially by altering focal adhesion-cytoskeleton assembly and display a different bone cell phenotype on nanoscale interfaces suggests that nanoscale substratum modification may be used for the control of cell functions.

We thank The Pennsylvania State Tobacco Settlement Formula Fund and The Pennsylvania State University Materials Research Institute for the support of this work. We thank Dr Zhiyi Zhou for providing hFOB cells.

REFERENCES

Affrossman, S. & Stamm, M. 2000 The effect of molecular weight on the topography of thin films of blends of poly(4-bromostyrene) and polystyrene. *Colloid Polym. Sci.* **278**, 888–893.

Affrossman, S., Henn, G., O'Neill, S. A., Pethrick, R. A. & Stamm, M. 1996 Surface topography and composition of deuterated polystyrene–poly(bromostyrene) blends. *Macromolecules* **29**, 5010–5016.

Affrossman, S., O'Neill, S. A. & Stamm, M. 1998 Topography and surface composition of thin films of blends of polystyrene with bromiated polystyrenes: effects of varying the degree of bromination and annealing. *Macromolecules* **31**, 6280–6288.

Alberts, B., Bray, D., Lewis, J., Raff, M., Roberts, K. & Watson, J. D. 1994 *Molecular biology of the cell*, 3rd edn. New York: Garland Publishing.

Al-Omari, W. M., Mitchell, C. A. & Cunningham, J. L. 2001 Surface roughness and wettability of enamel and dentine surfaces prepared with different dental burs. *J. Oral Rehabil.* **28**, 645–650.

Bico, J., Tordeux, C. & Quéré, D. 2001 Rough wetting. *Europhys. Lett.* **55**, 214–220.

Boyan, B. D., Hummert, T. W., Dean, D. D. & Schwartz, Z. 1996 Role of material surfaces in regulating bone and cartilage cell response. *Biomaterials* **17**, 137–146.

Britland, S., Morgan, H., Wojiak-Stodart, B., Riehle, M., Curtis, A. & Wilkinson, C. 1996 Synergistic and hierarchical adhesive and topographic guidance of BHK cells. *Exp. Cell Res.* **228**, 313–325.

Chen, C. S., Alonso, J. L., Ostuni, E., Whitesides, G. M. & Ingber, D. E. 2003 Cell shape provides global control of focal adhesion assembly. *Biochem. Biophys. Res. Commun.* **307**, 355–361.

Clark, P., Connolly, P., Curtis, A. S. G., Dow, J. A. T. & Wilkinson, C. D. W. 1987 Topographical control of cell behaviour: simple step cues. *Development* **99**, 439–448.

Clark, P., Connolly, P., Curtis, A. S. G., Dow, J. A. T. & Wilkinson, C. D. W. 1991 Cell guidance by ultrafine topography in vitro. *J. Cell Sci.* **99**, 73–77.

Dalby, M. J., Riehle, M. O., Johnstone, H. J. H., Affrossman, S. & Curtis, A. S. G. 2002*a* In vitro reaction of endothelial cells to polymer demixed nanotopography. *Biomaterials* **23**, 2945–2954.

Dalby, M. J., Yarwood, S. J., Riehle, M. O., Johnstone, H. J. H., Affrossman, S. & Curtis, A. S. G. 2002*b* Increasing fibroblast response to materials using nano-topography: morphological and genetic measurements of cell response to 13 nm high polymer demixed islands. *Exp. Cell Res.* **276**, 1–9.

Dalby, M. J., Childs, S., Riehle, M. O., Johnstone, H. J. H. & Affrossman, S. 2003 Fibroblast reaction to island topography: changes in cytoskeleton and morphology with time. *Biomaterials* **24**, 927–935.

Dalby, M. J., Gadegaard, N., Riehle, M. O., Wilkinson, C. D. & Curtis, A. S. G. 2004*a* Investigating filopodia sensing using arrays of defined nano-pits down to 35 nm diameter in size. *Int. J. Biochem. Cell Biol.* **36**, 2005–2015.

Dalby, M. J., Giannarasa, D., Riehle, M. O., Gadegaarda, N., Affrossman, S. & Curtis, A. S. G. 2004*b* Rapid fibroblast adhesion to 27 nm high polymer demixed nano-topography. *Biomaterials* **25**, 77–83.

Dalby, M. J., Riehle, M. O., Johnstone, H., Affrossman, S. & Curtis, A. S. G. 2004*c* Investigating the limits of filopodial sensing: a brief report using SEM to image the interaction between 10 nm high nano-topography and fibroblast filopodia. *Cell Biol. Int.* **28**, 229–236.

den Braber, E. T., de Ruijter, J. E., Smits, H. T. J., Ginsel, L. A., von Recum, A. F. & Jansen, J. A. 1996 Quantitative analysis of cell proliferation and orientation on substrata with uniform parallel surface micro-grooves. *Biomaterials* **17**, 1093–1099.

Donahue, H. J. 2000 Gap junctions and biophysical regulation of bone cell differentiation. *Bone* **26**, 417–422.

Donahue, H. J., Li, Z., Zhou, Z. & Yellowley, C. E. 2000 Differentiation of human fetal osteoblastic cells and gap junctional intercellular communication. *Am. J. Physiol. Cell Physiol.* **278**, C315–C322.

Ezzell, R. M., Goldmann, W. H., Wang, N., Parasharama, N. & Ingber, D. E. 1997 Vinculin promotes cell spreading by mechanically coupling integrins to the cytoskeleton. *Exp. Cell Res.* **231**, 14–26.

Flemming, R. G., Murphy, C. J., Abrams, G. A., Goodman, S. L. & Nealey, P. F. 1999 Effects of synthetic micro- and nano-structured surfaces on cell behavior. *Biomaterials* **20**, 573–588.

Giancotti, F. G. & Ruoslahti, E. 1999 Integrin signaling. *Science* **285**, 1028–1031.

Guckenbiehl, B., Stamm, M. & Springer, T. 1994 Interface properties of blends of incompatible polymers. *Physica B* **198**, 127–130.

Harris, S. A., Enger, R. J., Riggs, B. L. & Spelsberg, T. C. 1995 Development and characterization of a conditionally immortalized human fetal osteoblastic cell line. *J. Bone Miner. Res.* **10**, 178–186.

Hynes, R. 1992 Integrins: versatility, modulation and signaling in cell adhesion. *Cell* **69**, 11–25.

Lacouture, M. E., Schaffer, J. L. & Klicksten, L. B. 2002 A comparison of type I collagen, fibronectin, and vitronectin in supporting adhesion of mechanically strained osteoblasts. *J. Bone Miner. Res.* **17**, 481–492.

Langer, R. & Vacanti, J. P. 1993 Tissue engineering. *Science* **260**, 920–926.

Lim, J. Y., Liu, X., Vogler, E. A. & Donahue, H. J. 2004 Systematic variation in osteoblast adhesion and phenotype with substratum surface characteristics. *J. Biomed. Mater. Res. A* **68**, 504–512.

Lim, J. Y., Taylor, A. F., Li, Z., Vogler, E. A. & Donahue, H. J. 2005 Integrin expression and osteopontin regulation in human fetal osteoblastic cells mediated by substratum surface characteristics. *Tissue Eng.* **11**, 19–29.

Downloaded from rsif.royalsocietypublishing.org

Massia, S. P. & Hubbell, J. A. 1991 An RGD spacing of 440 nm is sufficient for integrin alpha V beta 3-mediated fibroblast spreading and 140 nm for focal contact and stress fiber formation. *J. Cell Biol.* **114**, 1089–1100.

Matsuzaka, K., Walboomers, F., de Ruijter, A. & Jansen, J. A. 2000 Effect of microgrooved poly-L-lactic (PLA) surfaces on proliferation, cytoskeletal organization, and mineralized matrix formation of rat bone marrow cells. *Clin. Oral Implants Res.* **11**, 325–333.

Meyle, J., Gultig, K., Brich, M., Hammerle, H. & Nisch, W. 1994 Contact guidance of fibroblasts on biomaterial surfaces. *J. Mater. Sci. Mater. Med.* **5**, 463–466.

Moursi, A. M., Globus, R. K. & Damsky, C. H. 1997 Interactions between integrin receptors and fibronectin are required for calvarial osteoblast differentiation in vitro. *J. Cell Sci.* **110**, 2187–2196.

Nealey, P. F. 1999 Effects of synthetic micro- and nano-structured surfaces on cell behavior. *Biomaterials* **20**, 573–588.

Oakley, C. & Brunette, D. M. 1995*a* Topographic compensation: guidance and directed locomotion of fibroblasts on grooved micromachined substrata in the absence of microtubules. *Cell Motil. Cytoskel.* **31**, 45–58.

Oakley, C. & Brunette, D. M. 1995*b* Response of single, pairs, and clusters of epithelial cells to substratum topography. *Biochem. Cell Biol.* **73**, 473–489.

Oakley, C., Jaeger, A. F. & Brunette, D. M. 1997 Sensitivity of fibroblasts and their cytoskeletons to substratum topographies: topographic guidance and topographic compensation by micromachined grooves of different dimensions. *Exp. Cell Res.* **234**, 413–424.

Öner, D. & McCarthy, T. J. 2000 Ultrahydrophobic surfaces. Effects of topography length scales on wettability. *Langmuir* **16**, 7777–7782.

Rajnicek, A. M. & McCraig, C. D. 1997 Guidance of CNS growth cones by substratum grooves and ridges: effects of inhibitors of the cytoskeleton, calcium channels and signal transduction pathways. *J. Cell Sci.* **110**, 2915–2924.

Rice, J. M., Hunt, J. A., Gallagher, J. A., Hanarp, P., Sutherland, D. S. & Gold, J. 2003 Quantitative assessment of the response of primary derived human osteoblasts and macrophages to a range of nanotopography surfaces in a single culture model in vitro. *Biomaterials* **24**, 4799–4818.

Riehle, M. O., Dalby, M. J., Johnstone, H., MacIntosha, A. & Affrossman, S. 2003 Cell behaviour of rat calvaria bone cells on surfaces with random nanometric features. *Mater. Sci. Eng. C* **23**, 337–340.

Rupp, F., Scheideler, L., Rehbein, D., Axmann, D. & Geis-Gerstorfer, J. 2004 Roughness induced dynamic changes of wettability of acid etched titanium implant modifications. *Biomaterials* **25**, 1429–1438.

Shirato, I., Tomino, Y., Koide, H. & Sakai, T. 1991 Fine structure of the glomerular basement membrane of the rat kidney visualized by high-resolution scanning electron microscopy. *Cell Tissue Res.* **266**, 1–10.

Svitkina, T. M., Bulanova, E. A., Chaga, O. Y., Vignjevic, D. M., Kojima, S., Vasiliev, J. M. & Borisy, G. G. 2003 Mechanism of filopodia initiation by reorganization of a dendritic network. *J. Cell Biol.* **160**, 409–421.

Teixeira, A. I., Abrams, G. A., Bertics, P. J., Murphy, C. J. & Nealey, P. F. 2003 Epithelial contact guidance on well-defined micro- and nanostructured substrates. *J. Cell Sci.* **116**, 1881–1892.

van Kooten, T. G., Whitesides, J. F. & von Recum, A. F. 1998 Influence of silicone (PDMS) surface texture on human skin fibroblast proliferation as determined by cell cycle analysis. *J. Biomed. Mater. Res.* **43**, 1–14.

Vogler, E. A. 1999 Water and the acute biological response to surfaces. *J. Biomater. Sci. Polym. Ed.* **10**, 1015–1045.

Walboomers, X. F., Croes, H. J., Ginsel, L. A. & Jansen, J. A. 1998 Growth behavior of fibroblasts on microgrooved polystyrene. *Biomaterials* **19**, 1861–1868.

Walboomers, X. F., Croes, H. J., Gensel, L. A. & Jansen, J. A. 1999 Contact guidance of rat fibroblasts on various implant materials. *J. Biomed. Mater. Res.* **47**, 204–212.

Wojciak-Stothard, B., Madeja, Z., Korohoda, W., Curtis, A. & Wilkinson, C. 1995 Activation of macrophage-like cells by multiple grooved substrata. Topographical control of cell behavior. *Cell Biol. Int.* **19**, 485–490.

Wojciak-Stothard, B., Curtis, A., Monaghan, W., MacDonald, K. & Wilkinson, C. 1996 Guidance and activation of murine macrophages by nanometric scale topography. *Exp. Cell Res.* **223**, 426–435.

Yap, A. S. & Kovacs, E. M. 2003 Direct cadherin-activated cell signaling: a view from the plasma membrane. *J. Cell Biol.* **160**, 11–16.